ARTICLES

Supramolecular Catalysts for the Gas-phase Synthesis of Single-walled Carbon Nanotubes

Takeshi Saito,*,† Wei-Chun Xu,‡ Satoshi Ohshima,† Hiroki Ago,†,§ Motoo Yumura,† and Sumio Iijima†

Research Center for Advanced Carbon Materials, National Institute of Advanced Industrial Science and Technology (AIST), Tsukuba 305-8565, Japan, Kashiwa Laboratory, Institute of Research and Innovation (IRI), Kashiwa 277-0861, Japan, and Institute for Materials Chemistry and Engineering, Kyushu University, Kasuga 816-8580, Japan

Received: December 26, 2005; In Final Form: February 7, 2006

Reversed micelles containing metallic ions have been used as precursors of novel catalysts for the gas-phase synthesis of single-walled carbon nanotubes (SWNTs). This technique possesses the following advantages: (i) excellent solubility in organic solvents, which are used as reactants and (ii) facile preparation of multicomponent catalysts enabling systematic screening of catalyst compositions for the synthesis of SWNTs. In this study, we report the results of the screening study on the catalytic behavior of Fe−Mo binary catalysts during the synthesis of SWNTs. The results suggested that the catalytic ability was closely related to the strain of the crystal structure of Fe−Mo catalysts formed in the reaction and/or the phase transition caused by dissolution of the Mo atoms. The addition of lithium to the Fe−Mo binary catalysts has revealed an increase in the yield of SWNTs.

1. Introduction

Since their discovery in 1993,[1,2] a considerable amount of research focusing on synthesis methods and catalysts for single-walled carbon nanotubes (SWNTs) has been carried out.[3] In particular, the recent progress in the research of the chemical vapor deposition (CVD) method for the production of SWNTs[4−8] on a large scale, with low cost, and high quality has been outstanding. The CVD process for synthesizing SWNTs can be divided into two categories—one that uses catalysts supported on substrates or embedded in porous inorganic materials and the other that is a gas-phase growth as in the HiPco process.[4,5] The former is suitable for the fabrication of on-tip devices such as nanotube transistors, while the latter is believed to be an ideal continuous process for the production of SWNTs on a commercial scale.

The gas-phase growth of SWNTs is achieved by passing a mixed flow of organometallic catalyst precursors and carbon sources through a heated furnace reactor.[4,7,9−11] Recently, we have developed a simple and rational method, termed the direct-injection pyrolytic synthesis (DIPS) method for the gas-phase production of SWNTs. In this method, a toluene solution of nanoparticle catalysts is directly injected into a vertical reactor through a spray nozzle.[12,13] We found that a highly soluble catalyst is extremely important in this method for the high-yield production of SWNTs.[12] On the other hand, it is generally difficult to concentrate metal nanoparticles in organic solvents because high concentration causes flocculation of the nanoparticles. From this viewpoint, the development of a catalyst with excellent solubility in organic solvents is essential for the economic large-scale production of SWNTs by the DIPS method.

In this study, we propose a novel efficient catalyst—supramolecular catalyst—in order to realize the large-scale production of SWNTs, as illustrated in Figure 1. We have employed one of the simplest supramolecules, that is, reversed micelles, as the catalyst in the DIPS method. The reversed micelle, formed by the self-assembly of surfactants in apolar solvents, has uniform and spherical solution structures with nanoscale diameters. In other words, the supramolecular catalysts are liquid nanoparticles. There is a water pool in the core of the reversed micelle structure in which an abundant amount of water-soluble materials, such as iron and cobalt chlorides, can be confined. As compared with the other catalysts, supramolecular catalysts permit an abundant dissolution of metal catalysts; moreover, they enable the facile preparation of various multicomponent catalysts. This enables a systematic screening of catalyst compositions for the SWNTs synthesis. In this study, we have investigated the catalytic activity of supramolecular catalysts comprising iron−molybdenum (Fe−Mo) with different compositions in the gas-phase growth of SWNTs by the DIPS method.

2. Experimental Section

The supramolecular catalysts were prepared in a glovebox filled with nitrogen gas because surfactants and metal chloride reagents are extremely hygroscopic. The typical procedure is as follows: 15.0 mmol of dimethyldioctylammonium bromide (Tokyo Kasei Kogyo Co., Ltd., Japan) was dissolved in 10 g of toluene (Wako Pure Chemical Industries, Ltd., Japan). In

* To whom correspondence should be addressed. E-mail: takeshi-saito@aist.go.jp. Tel: +81-29-861-4863. Fax: +81-29-861-3392.
† AIST.
‡ IRI.
§ Kyushu University.

10.1021/jp057513i CCC: $33.50
Published on Web 03/07/2006

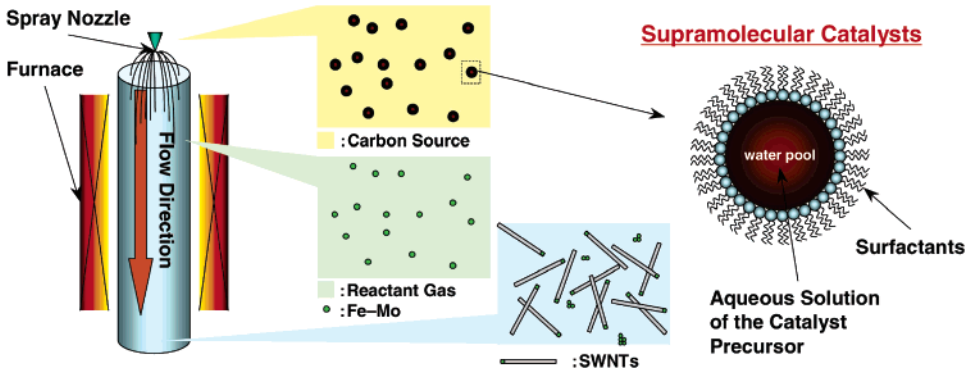

Figure 1. Schematic representation of the gas-phase synthesis of SWNTs by using supramolecular catalysts. Starting material, comprising supramolecular catalysts and organic solvent as the carbon source, was directly injected into a vertical reactor through a spray nozzle. In the reactor, the supramolecular catalysts sinter to form the nanoparticles which then function as catalysts for growing SWNTs. The product flowed out of a hot zone of the reactor with the carrier gas stream.

this solution, 7.86 mmol of anhydrous iron(III) chloride and 0.981 mmol of molybdenum chloride were dissolved and sonicated to make the solution homogeneous. This solution was centrifuged at 5390 × g for 10 min in order to remove precipitate. Prior to the gas-phase synthesis of SWNTs by the DIPS method, an equimolar amount of thiophene against iron atoms was added to the supernatant solution as a promoter to obtain the starting material.

The detailed experimental procedures for the CVD synthesis of SWNTs by the DIPS method are described elsewhere.[13] In brief, the above-mentioned starting material was supplied directly to a vertical quartz tube reactor through a spray nozzle with a microfeeder at a rate of 64 μL/min under a hydrogen carrier gas flow of 7000 sccm. The reaction temperature of the furnace was set at 1200 °C, and the flange at the top of the quartz tube where the spray was attached was cooled below 100 °C. The inner diameter of the quartz tube was 50 mm, and the length of the reactor was 600 mm. On the basis of the volume of the carrier gas at 1200 °C, the residence time in the reactor can be derived to be ca. 2.1 s. Therefore, the reaction time of each nanoparticle of a catalyst was estimated to be less than 2.1 s at the above-mentioned condition. The as-grown product (SWNTs) was caused to flow out of the hot zone of the reactor by the hydrogen carrier gas stream and collected at the bottom of the reactor using a stainless steel mesh filter. The duration of the reaction was 60 min. Large quantities of weblike and very light carbon materials were obtained from the reaction.

Synthesized carbon products were characterized by scanning electron microscopy (SEM) (Hitachi S-5000) and transmission electron microscopy (TEM) (JEOL JEM1010). The resonance Raman scattering spectra were measured using a triple-monochromator micro-Raman spectrometer (JASCO NRS-2100) in a backscattering configuration. We adopted an argon-ion laser operating at 488 or 514.5 nm and a krypton-ion laser operating at 647 nm as the excitation laser line.

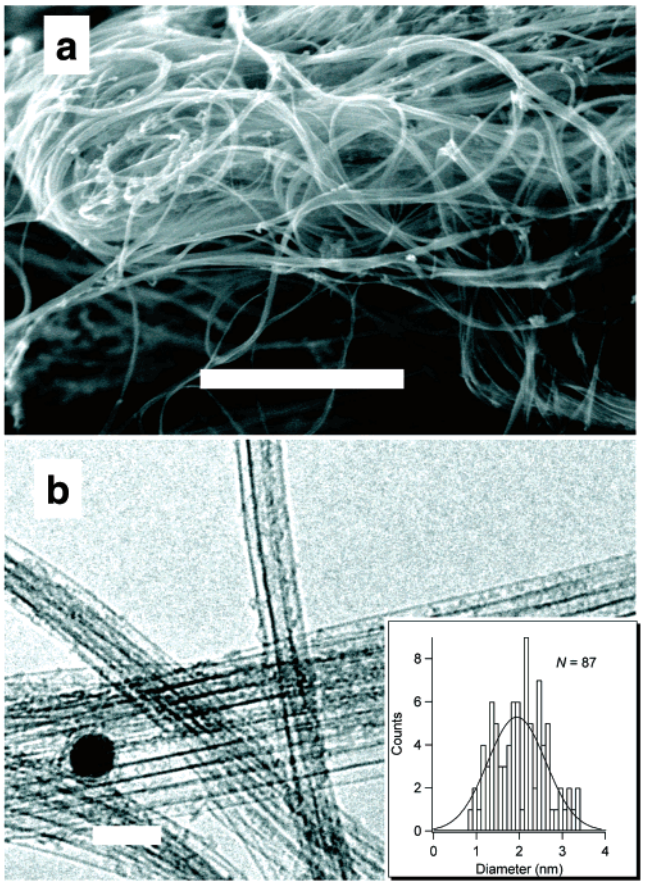

Figure 2. Typical SEM (a) and TEM images (b) of the as-grown SWNTs obtained by the DIPS method using the supramolecular catalysts with an Fe/Mo ratio of 0.125. High densities of entangled SWNTs filaments were observed. The scale bars in (a) and (b) represent 1 μm and 10 nm, respectively.

3. Results and Discussion

Typical SEM and TEM images of the carbon product collected on the mesh filter are shown in Figure 2. These images show entangled SWNTs, which are homogeneously distributed over large areas. On the basis of the TEM images, we obtained a histogram of SWNT diameters, as shown in the inset of Figure 2b. By Gaussian fitting, we estimated the average diameter to be 1.9 ± 0.96 nm.

The resonance Raman scattering spectra measured in the frequency regions of 1250−1700 and 55−300 cm^{-1} are shown in parts a and b of Figure 3, respectively. The remarkable feature in Figure 3a is that the peaks assigned to the disorder-induced mode (D-band) are extremely weak, implying that there are relatively few amorphous carbon impurities and defects in the graphene structure of the SWNTs[14,15] produced. This could be attributed to the high reaction temperature employed in the process. The Raman peaks observed in the low-frequency region are assigned to radial breathing mode (RBM) vibration (Figure 3b) of SWNTs; this corresponds to the atomic vibration of carbon atoms in the radial direction as if the tube was breathing. On the basis of the RBM peaks, we can estimate the SWNT diameter from the experimental relationship, $d = 248/\omega_{RBM}$,[16] where ω_{RBM} is the RBM vibration frequency observed and d is

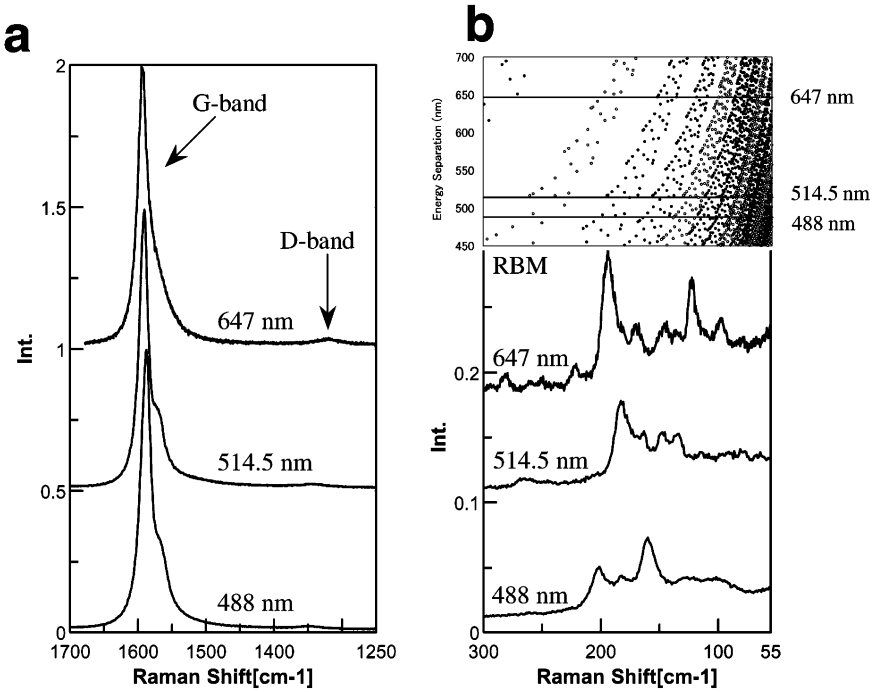

Figure 3. Raman spectra were recorded in the range of 1250−1700 cm^{-1} (a) and from 55 to 300 cm^{-1} (b) of the as-grown SWNTs. An Ar-ion laser (488 and 514.5 nm) and a Kr-ion laser (647 nm) were used. The corresponding Kataura plot of resonance wavelength vs RBM frequency is also represented in (b).

the tube diameter. It is apparent that the resonance Raman measurement with a single laser line is inadequate for measuring the diameter distribution of the SWNTs sample. This is because such a measurement only reveals the resonance condition of the tubes with the application of a laser line wavelength. A good characterization of the diameter distribution in the SWNTs can be obtained by measuring the Raman spectra using many laser lines. In the present study, we used three laser lines—488, 514.5, and 647 nm—to measure the tube−diameter distribution. In Figure 3b, the Raman scattering spectra with the RBM peaks are shown, together with the Kataura plot[17] of the resonance wavelength vs the RBM frequency. A majority of the RBM peaks were observed in the range of ca. 100−200 cm^{-1}, which corresponds to the diameter range of 1.2−2.5 nm, according to the above-mentioned relation. It should be noted that this range is approximately consistent with the diameter histogram evaluated from the TEM observation, as shown in the inset of Figure 2b. The SWNTs with relatively large diameters that utilize the encapsulation of the included molecules appear to be a promising candidate for gas-storage[7] and device applications such as peapods (fullerene-encapsulated SWNTs).

As mentioned above, the supramolecular catalysts enable the systematic screening of multicomponent catalysts to be carried out. On this basis, we investigated the effect of the composition of Fe−Mo bimetallic catalysts on the formation of SWNTs. Several supramolecular catalyst solutions with different Mo/Fe ratios ranging from 0 to 0.20 were prepared and used as the starting materials in the gas-phase growth of SWNTs by the DIPS method. Further, only the amount of molybdenum chloride was changed systematically, and the toluene, surfactant, and iron chloride amounts were set as constant during the preparation of the catalysts. The yield of SWNTs against the Mo/Fe ratio was plotted in Figure 4a. This yield was defined as the mass of the raw carbon product produced per hour. To reduce the experimental error, the experiments were carried out three times under the same reaction conditions and each plotted value of the yield represents the average of the three experiments. It

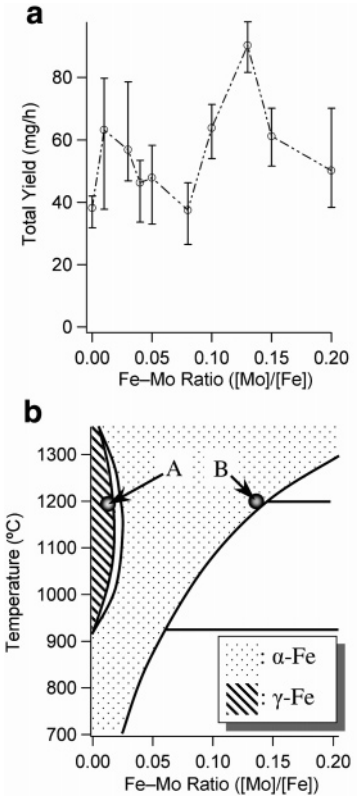

Figure 4. Correlation between the Mo/Fe ratio and the catalytic ability. (a) SWNTs yield against the Fe/Mo ratio. The amounts of toluene, surfactant, and iron chloride in the starting materials were maintained constant while the amount of molybdenum chloride was varied in the preparation of catalysts. (b) The Fe−Mo binary alloy phase diagram. The abscissa is in the Fe/Mo ratio.

should be noted that, to investigate the activity of the different catalysts based on their yields, the content of SWNTs should be almost identical among all the samples. We carried out thermal analysis studies—thermogravimetric analysis (TGA) and

differential thermal analysis (DTA)—to check the SWNT contents in the raw carbon product. This result is presented in the Supporting Information. The result of TGA showed that the carbon contents were almost identical (ca. 80 at. %) within the experimental error among all our products. In the DTA plot, two large peaks indicating exothermic change were observed at 370 and 480 °C. On the other hand, weight gain and loss in the TGA plot were also observed around 370 and 480 °C, respectively. According to these results, the two peaks in the DTA plot at 370 and 480 °C could be attributed to the oxidation of iron catalysts and SWNTs, respectively. Further, in the CVD synthesis, we can estimate that the major product using the DIPS method is SWNT. As shown in Supporting Information S3, the Raman spectra recorded in these samples also supported the fact that the qualities of the samples are almost identical. Thus, we can safely discuss the activity of the catalysts based on their yields in the range of the present Mo/Fe ratio.

In Figure 4a, we observe that there is a small peak at the Mo/Fe ratio = 0.0125 and a larger peak at 0.125. The increase in the yield of SWNTs can be attributed to the synergistic effects between Fe and Mo being similar to that observed in the cobalt−molybdenum (CoMo) catalyst system.[18,19] This synergistic effect and the role of Mo have been reported in detail for CoMo-supported catalysts and two possible explanations were proposed: Mo stabilizes nanoparticles with 1−2 nm diameters and/or acts as a carbon supplier. Interestingly, it was found that the Mo/Fe ratios of 0.0125 and 0.125 approximately correspond to specific points A and B, respectively, in the Fe−Mo binary alloy phase diagram shown in Figure 4b.[20] In this binary alloy system, points A and B correspond to the regions of maximum dissolvable amounts of Mo atoms in the γ- and α-Fe phases, respectively. A comparison between the dependence of the yield of SWNTs on Mo/Fe and a phase diagram suggests that the catalytic ability is closely related with the strain of the crystal structure and/or the phase transition caused by the dissolution of Mo atoms. If this supposition is true, then it can be considered that the Mo/Fe ratio that causes a maximum yield of SWNTs at reaction temperatures lower than 1200 °C should decrease below 0.125. This is because the maximum dissolvable amount of Mo in the α-Fe phase decreases with temperature (see Figure 4b). In fact, the increase in the yield of SWNTs was confirmed at a Mo/Fe ratio of 0.08 when the reaction temperature was reduced to 1100 °C.

We further discuss the validity of applying the phase diagram to our catalysts. In this case, the size of the catalyst particles formed in the reactor appears important. Recently, Nasibulin et al.[21] have reported the effect of the catalyst particle size and the experimental conditions on the diameter of the SWNTs formed by the gas phase. They have pointed out that there is a large discrepancy between the sizes of catalyst particles and the diameter of SWNTs. Further, they experimentally proved that the ratio of catalyst particle size to the SWNT diameters ([particle size]/[tube diameter]) is ca. 1.6, independent of the experimental conditions. In accordance with this result, the size of the catalyst particles formed in the reactor can be deduced to be ca. 1.5−5.6 nm from the diameter distribution of the SWNTs (0.9−3.5 nm) obtained in the present study. Therefore, each particle would contain ca. 200−16 000 metal atoms. When the particle size is 3.2 nm deduced from the average diameter of the SWNTs, each particle contains ca. 1650 atoms and the surface atoms of the particle can be estimated to be ca. 25%. This suggests that the nanoparticle catalysts adopted are not extremely small and exhibit a crystal habit as reported in gold nanoclusters.[22] Furthermore, the phase transition from the α-Fe to γ-Fe phase was observed even in the case of an iron nanocluster.[23] Therefore, although the melting point of our nanoparticle catalyst is somewhat lower than that of bulk materials, the phase diagram can still be used for explaining our results.

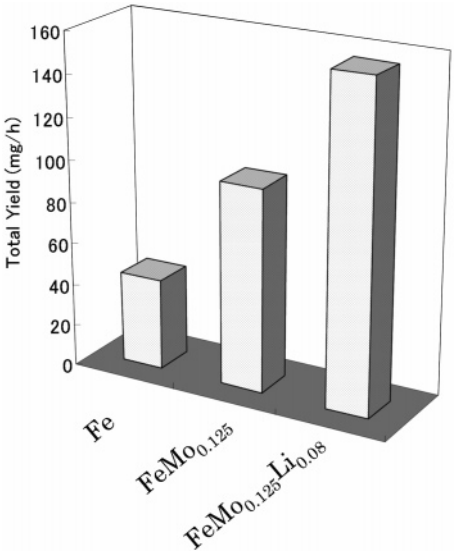

Figure 5. Yields of the carbon product obtained from Fe, Fe−Mo, and Fe−Mo−Li catalysts.

To demonstrate the validity of our supramolecular catalysts, we have studied a third component in addition to Fe−Mo and found that the addition of lithium (Li) improves the growth yield, as shown in Figure 5. This is probably due to the effect of the increased strain in the crystal structure of the Fe−Mo alloy induced by the dissolution of the Li atoms. We also observed that the preparation of high-concentration supramolecular catalysts for the high-yield production of SWNTs was fairly simple. We have prepared the above-mentioned Fe−Mo−Li catalyst solution with a concentration two times higher. With this as the starting solution, the gas-phase synthesis was carried out four times and the average yield was 286.5 mg/h; this is ca. 100 times greater than that of our recent study using solid metal nanoparticle catalysts.[12]

4. Conclusion

We have utilized reversed micelles as a precursor of the novel catalysts—supramolecular catalysts—for the gas-phase synthesis of SWNTs. We investigated the screening study of the catalyst composition in the Fe−Mo binary alloy catalyst system and found that there exists a correlation between catalytic ability and the Fe−Mo binary alloy phase diagram. This result suggests that the catalytic ability is closely related to the strain of the crystal structure and/or the phase transition caused by the dissolution of Mo atoms. Furthermore, we have found that a small amount of Li effectively improved the yield of SWNTs.

To the best of our knowledge, generally, the screening study of the multicomponent catalysts cannot be realized efficiently by using organometallic catalyst precursors or ordinary metal nanoparticle catalysts. These screening studies using the supramolecular catalysts are expected to contribute to the future development of more efficient multicomponent catalysts and the elucidation of the detailed mechanism of the catalytic synthesis of SWNTs.

Acknowledgment. This work is partially supported by the Nano Carbon Technology (NCT) project of the Ministry of

Economy, Trade and Industry (METI), Japan. The authors thank Ms. Y. Saito for the experimental assistance.

Supporting Information Available: The result of the catalyst size analysis is shown in S1. The results of the thermal analyses (TGA/DTA) are shown in S2. The Raman spectra of SWNTs synthesized by using various Fe−Mo supramolecular catalysts are shown in S3. The Raman spectrum of SWNTs synthesized by using Fe−Mo−Li supramolecular catalysts is shown in S4. This material is available free of charge via the Internet at http://pubs.acs.org.

References and Notes

(1) Iijima, S.; Ichihashi, T. *Nature* **1993**, *363*, 603−605.

(2) Bethune, D. S.; Kiang, C. H.; de Vries, M. S.; Gorman, G.; Savoy, R.; Vazquez, J.; Beyers, R. *Nature* **1993**, *363*, 605−607.

(3) Tanaka, K.; Yamabe, T.; Fukui, K., Eds. *The Science and Technology of Carbon Nanotubes*; Elsevier: Oxford, U.K., 1999.

(4) Nikolaev, P.; Bronikowski, M. J.; Bradley, K.; Rohmund, F.; Colbert, D. T.; Smith, K. A.; Smalley, R. E. *Chem. Phys. Lett.* **1999**, *313*, 91−97.

(5) Bronikowski, M. J.; Williams, P. A.; Colbert, D. T.; Smith, K. A.; Smalley, R. E. *J. Vac. Sci. Technol., A* **2001**, *19*, 1800−1805.

(6) Cheng, H. M.; Li, F.; Su, G.; Pan, H. Y.; He, L. L.; Sun, X.; Dresselhaus, M. S. *Appl. Phys. Lett.* **1998**, *72*, 3282−3284.

(7) Cheng, H. M.; Li, F.; Sun, X.; Brown, S. D. M.; Pimenta, M. A.; Marucci, A.; Dresselhaus, G.; Dresselhaus, M. S. *Chem. Phys. Lett.* **1998**, *289*, 602−610.

(8) Hata, K.; Futaba, D. N.; Mizuno, K.; Namai, T.; Yumura, M.; Iijima, S. *Science* **2004**, *306*, 1362−1364.

(9) Endo, M. *CHEMTECH* **1988**, *18*, 568−576.

(10) Tibbetts, G. G.; Bernardo, C. A.; Gorkiewicz, D. W.; Alig, R. L. *Carbon* **1994**, *32*, 569−576.

(11) Satishkumar, B. C.; Govindaraj, A.; Sen, R.; Rao, C. N. R. *Chem. Phys. Lett.* **1998**, *293*, 47−52.

(12) Ago, H.; Ohshima, S.; Uchida, K.; Yumura, M. *J. Phys. Chem. B* **2001**, *105*, 10453−10456.

(13) Saito, T.; Ohshima, S.; Xu, W.-C.; Ago, H.; Yumura, M.; Iijima, S. *J. Phys. Chem. B* **2005**, *109*, 10647−10652.

(14) Jorio, A.; Pimenta, M. A.; Filho, A. G. S.; Saito, R.; Dresselhaus, G.; Dresselhaus, M. S. *New J. Phys.* **2003**, *5*, 139.

(15) Jorio, A.; Fantini, C.; Dantas, M. S. S.; Pimenta, M. A.; Filho, A. G. S.; Samsonidze, G. G.; Brar, V. W.; Dresselhaus, G.; Dresselhaus, M. S.; Swan, A. K.; Ünlü, M. S.; Goldberg, B. B.; Saito, R. *Phys. Rev. B* **2002**, *66*, 1154111−1154118.

(16) Jorio, A.; Saito, R.; Hafner, J. H.; Lieber, C. M.; Hunter, M.; McClure, T.; Dresselhaus, G.; Dresselhaus, M. S. *Phys. Rev. Lett.* **2001**, *86*, 1118−1121.

(17) Kataura, H.; Kumazawa, Y.; Maniwa, Y.; Umezu, I.; Suzuki, S.; Ohtsuka, Y.; Achiba, Y. *Synth. Met.* **1999**, *103*, 2555−2558.

(18) Alvarez, W. E.; Kitiyanan, B.; Borgna, A.; Resasco, D. E. *Carbon* **2001**, *39*, 547−558.

(19) Hu, M.; Murakami, Y.; Ogura, M.; Maruyama, S.; Okubo, T. *J. Catal.* **2004**, *225*, 230−239.

(20) Massalski, T. B.; Okamoto, H.; Subramanian, P. R.; Kacprzak, L. *Binary Alloy Phase Diagrams*, 2nd ed.; ASM International: Materials Park, OH, 1990.

(21) Nasibulin, A. G.; Piknitsa, P. V.; Jiang, H.; Kauppinen, E. I. *Carbon* **2005**, *43*, 2251−2257.

(22) Iijima, S.; Ichihashi, T. *Jpn. J. Appl. Phys.* **1985**, *24*, L125-L128.

(23) Kusunoki, M.; Ichihashi, T. *Jpn. J. Appl. Phys.* **1986**, *25*, L219-L221.